Published in final edited form as:
Neuron. 2014 October 1; 84(1): 107–122. doi:10.1016/j.neuron.2014.09.012.

Experience-dependent remodeling of basket cell networks in the dentate gyrus

Simon Pieraut[1,2], **Natalia Gounko**[1,2,&], **Richard Sando III**[1,2,3], **Westley Dang**[1,2,3], **Elisabeth Rebboah**[1,2], **Satchidananda Panda**[4], **Linda Madisen**[5], **Hongkui Zeng**[5], and **Anton Maximov**[1,2,*]

[1]Department of Molecular and Cellular Neuroscience, The Scripps Research Institute, La Jolla, CA 92037, USA

[2]The Dorris Neuroscience Center, The Scripps Research Institute, La Jolla, CA 92037, USA

[3]The Kellogg School of Science and Technology, The Scripps Research Institute, La Jolla, CA 92037, USA

[4]Regulatory Biology Laboratory. The Salk Institute for Biological Studies, La Jolla, CA 92037, USA

[5]Allen Institute for Brain Science, Seattle, WA 98103, USA

SUMMARY

The structural organization of neural circuits is strongly influenced by experience, but the underlying mechanisms are incompletely understood. We found that, in the developing dentate gyrus (DG), excitatory drive promotes the somatic innervation of principal granule cells (GCs) by parvalbumin (PV)-positive basket cells. By contrast, presynaptic differentiation of GCs and interneuron sub-types that inhibit GC dendrites is largely resistant to loss of glutamatergic neurotransmission. The networks of PV basket cells in the DG are regulated by vesicular release from projection entorhinal cortical neurons and, at least in part, by NMDA receptors in interneurons. Finally, we present evidence that glutamatergic inputs and NMDA receptors regulate these networks through a presynaptic mechanism that appears to control the branching of interneuron axons. Our results provide insights into how cortical activity tunes the inhibition in a subcortical circuit, and reveal new principles of interneuron plasticity.

*To whom correspondence should be addressed: amaximov@scripps.edu.
&Present address: Joint IMB-IMCB Electron Microscopy Suite, A-Star, Singapore (20 Biopolis Street, #B2-14 Matrix Singapore 138671)

SUPPLEMENTAL MATERIALS with extended methods are attached to the manuscript.

INTRODUCTION

Virtually all circuits in the mammalian cortex and hippocampus recruit multiple sub-types of GABAergic interneurons that innervate the somato-dendritic axes of principal cells with remarkable selectivity and play unique physiological roles (DeFelipe et al., 2013; Fishell and Rudy, 2011; Isaacson and Scanziani, 2011; Tricoire et al., 2011). Increasing evidence suggests that the architectures of inhibitory networks are dynamically regulated by spontaneous and correlated activity. Intrinsic excitability is necessary for interneuron migration and differentiation, whereas neurotransmission driven by sensory stimuli promotes the development of GABAergic terminals and their redistribution in the adult brain (Bortone and Polleux, 2009; Chen et al., 2012; De Marco Garcia et al., 2011; Keck et al., 2011; Kullmann et al., 2012; van Versendaal et al., 2012). Experience-dependent changes in inhibitory synapse numbers involve synthesis of GABA, induction of the transcription factor, Npas4, and BDNF signaling (Chattopadhyaya et al., 2007; Lin et al., 2008; Spiegel et al., 2014). Moreover, cortical and hippocampal interneurons appear to have non-uniform propensities for re-wiring, which likely reflects their genetic diversity. Among these subtypes, parvalbumin (PV)-positive basket cells have emerged as one of the primary substrates for plasticity associated with learning (Bloodgood et al., 2013; Donato et al., 2013).

Despite these advances, some principles of structural plasticity of inhibitory networks are incompletely understood. Interneurons are reciprocally connected with glutamatergic neurons in circuits that process different kinds of sensory information incoming at various frequencies. They also mediate inhibition in a feedback and feedforward manner following excitatory inputs from local sources and long-range projections such as thalamic fibers in the cortex and cortical fibers in the hippocampus (Bagnall et al., 2011; Basu et al., 2013; Poo and Isaacson, 2009; Wehr and Zador, 2003; Wilent and Contreras, 2005). This opens possibilities for regulation of synapse numbers by pre- and postsynaptic signals of distinct cellular origin, but the involvement and potential interplays between these signals are relatively unexplored. It is also unclear how activity in a given circuit influences the morphologies of GABAergic axons which usually terminate onto numerous neighboring neurons. Loss of excitability and GABA synthesis has been shown to delay axon growth in cortical basket cells, while glutamate receptor antagonists produced similar effects in reelin- and calretinin-positive interneurons (Chattopadhyaya et al., 2004; Chattopadhyaya et al., 2007; De Marco Garcia et al., 2011). Consistent with these findings, remodeling of branch tips of broadly labeled interneurons has been observed in the visual cortex of sensory-deprived mice (Chen et al., 2011). Yet, these experimental paradigms do not identify the sources of synaptic release that guide axon branching.

In the present study, we combined genetic approaches with imaging and electrophysiology to determine how vesicular release and NMDA receptors affect neuronal connectivity in the developing dentate gyrus (DG). In this gateway to the hippocampus, granule cells (GCs) relay information essential for pattern separation and spatial memory from the entorhinal cortex (EC) to the CA3 (Figure 1A) (Forster et al., 2006; Nakashiba et al., 2012). The coding in the DG is sparse, at least in part due to strong inhibition that filters uncorrelated noise (Acsady and Kali, 2007; Treves et al., 2008). Like other classes of glutamatergic

neurons, GCs are innervated by a diverse group of interneurons whose synaptic terminals are strictly laminated (Houser, 2007). Here, we discuss findings that provide insights into the role of cortical activity in tuning the GABAergic inhibition in the DG at a structural level and reveal new mechanisms that may control the presynaptic networks of basket cells across the forebrain.

RESULTS

Anatomical characterization of mice expressing TeNT in glutamatergic neurons

The majority of new synapses are formed in the DG during early postnatal development followed by gradual incorporation of adult-born GCs into preexisting networks (Forster et al., 2006). To investigate how connectivity between GCs and other neuron types depends on synaptic transmission, we first globally reduced excitatory drive in the cortex and hippocampus of juvenile mice. This was accomplished via expression of tetanus toxin (TeNT), a protease that blocks vesicular release by cleaving a SNARE, synaptobrevin/VAMP2 (Syb2) (Schoch et al., 2001). TeNT was introduced into glutamatergic neurons throughout the forebrain using previously described CamKIIα:Cre and Cre-inducible $R26^{floxstop\text{-}TeNT}$ alleles (Sando et al., 2012; Saura et al., 2004; Zhang et al., 2008) (Figure 1B). In parallel, we defined the time-course of CamKIIα:Cre induction by monitoring the Ai9 tdTomato reporter (Madisen et al., 2010). The fractions of reporter-positive cells progressively increased after birth approaching the plateau by postnatal (P) day 21 (Figure S1A–C). Consistent with these results, CamKIIα:Cre/$R26^{floxstop\text{-}TeNT}$ mice began to exhibit reduced locomotion at P14, and did not survive past P21.

Given the restricted lifespan of CamKIIα:Cre/$R26^{floxstop\text{-}TeNT}$ mutants we interrogated them at P14, when recombination in the EC and DG reaches the midpoint. These animals had normal morphology of the hippocampus with unaltered distribution of differentiating and mature GCs in the DG. Furthermore, imaging of large mossy fiber terminals (LMTs) labeled with an antibody to synaptic vesicle protein, synaptoporin (SPO), showed that gross patterning of GC axons was preserved (Figures 1C–D and S1D–G). As expected, expression of TeNT led to a ~40–60% reduction in the numbers of GCs immunoreactive for Zif268 and cFos, the products of immediate early genes whose transcription is coupled with neuronal activity. We also observed a ~2-fold decrease in the density of puncta with detectable Syb2 in the molecular layer (ML) of the DG, hilus and CA3, which confirms a proteolytic cleavage and depletion of Syb2 from neurotransmitter vesicles of glutamatergic synapses (Figure 1E–F and data not shown).

Loss of excitatory drive in the EC-DG-CA3 pathway leads to reduced inhibition of GCs

The DG receives robust glutamatergic inputs from pyramidal neurons located in layer 2 of the entorhinal cortex (EC2) whose axons terminate on dendrites of GCs in the ML (Forster et al., 2006; van Groen et al., 2003). To evaluate the physiological consequences of TeNT expression, we monitored neurotransmission in acute brain slices. Spontaneous excitatory postsynaptic currents (sEPSCs) and evoked responses (eEPSCs) to extracellular stimulation of the perforant path were sampled from mature GCs in whole-cell mode. In agreement with quantifications of recombination in the EC and Zif268, cFos and Syb2 immunoreactivity in

the DG, CamKIIα:Cre/R26$^{floxstop\text{-}TeNT}$ mice had a ~2-fold reduction in the frequency of AMPA-type sEPSCs. Likewise, the amplitudes of AMPA- and NMDA-type eEPSCs were smaller in these animals by ~2-fold (Figure 1G–H). We then recorded inhibitory postsynaptic currents (IPSCs) to assess the strength of inputs to GCs from GABAergic interneurons. In this case, synchronous GABA release was triggered by stimulation of the granule cell layer (GCL) where interneuron axons intermingle with GCs. Mutants carrying TeNT had lower frequencies of sIPSCs (~35%) and amplitudes of evoked eIPSCs (~4-fold), indicating that spontaneous and correlated inhibition of their GCs was also diminished (Figure 1I–J).

Owing to the specificity of Cre used to induce TeNT in CamKIIα:Cre/R26$^{floxstop\text{-}TeNT}$ mutants, this loss of inhibitory synaptic strength is likely associated with the blockade of vesicular release of glutamate (Figure S1H). Dentate interneurons are excited by GCs and projection EC neurons (Sambandan et al., 2010; Zipp et al., 1989), suggesting that either one or both glutamatergic cell types are involved. The downstream mechanisms may affect interneuron connectivity or orchestrate homeostatic scaling of functional synapses, as observed previously in other circuits (Bloodgood et al., 2013; Chen et al., 2012; Maffei et al., 2004; van Versendaal et al., 2012). However, the less attractive scenario of a broad delay in neuron differentiation cannot be ruled out. To begin to distinguish between these possibilities, we examined the structures of genetically-labeled GCs and further evaluated their physiological properties. A second rationale for these experiments is that our results are inconsistent with a recent study proposing that weakened GC mossy fibers are eliminated in a competitive environment (Yasuda et al., 2011). Because uniform counting of SPO-positive terminals formed by axons of intact and silenced GCs may be misleading, we wished to address this discrepancy with a more definitive approach.

GCs are largely tolerant to inactivity at a structural level

We targeted GCs of CamKIIα:Cre/R26$^{floxstop\text{-}TeNT}$ mice *in vivo* with adeno-associated virus that encodes a membrane-bound form of GFP (AAV2.2 DIO-mGFP). When delivered into the cerebral lateral ventricles, AAV2.2 preferentially transduces mature GCs (Burger et al., 2004). The virus transcribed mGFP in a Cre-inducible manner, allowing for selective tagging of neurons that express TeNT (Figures 2A and S2A–D). Animals were injected at P1 using a protocol that results in labeling of ~10% of GCs. Subsequently, these cells were inspected at P14 by confocal imaging of mGFP fluorescence in fixed sections and by whole-cell recordings in acute slices. Analysis of 3D-reconstructions of dendritic trees revealed no differences in the orientation and numbers of branches and nodes, the length of individual segments, and total dendrite length (Figures 2B–C and S2E–F). Notably, CamKIIα:Cre/R26$^{floxstop\text{-}TeNT}$ mice had ~20% less spines on GC dendrites, but the relative abundances of distinct spine types were unaltered. Also, mGFP-tagged neurons had normal intrinsic electrical properties and amplitudes of spontaneous postsynaptic currents, which rules out aberrant expression of voltage-gated ion channels and neurotransmitter receptors due to homeostatic adaptation to inactivity (Figures 2D–G and S2G–J). Finally, imaging of GC axons and LMTs in the hilus and CA3 showed that silenced mossy fibers developed at a normal rate and remained stable (Figure 2H–J). These results imply that GCs are largely

tolerant to silencing, and the loss of GABAergic input to these cells must be due to changes of the local inhibitory circuitry.

Synaptic excitation regulates the numbers of GABAergic synapses on GC somas

GCs are innervated by interneurons with different morphologies, firing rates and transcriptional profiles (Hosp et al., 2014; Houser, 2007; Tricoire et al., 2011). These include PV-positive fast spiking basket cells that mediate somatic inhibition, as well as calretinin (CR) and somatostatin (SST)-expressing neurons that form synapses on proximal and distal segments of GC dendrites in the supragranular zone (SZ) and ML, respectively (Figure 3A). To determine how excitatory neurotransmission influences the patterning of GABAergic synapses in this circuit, we initially imaged brain sections labeled with antibodies against native interneuron markers. CamKIIα:Cre/R26$^{floxstop\text{-}TeNT}$ mice had a ~2-fold lower density of GAD67-positive presynaptic terminals surrounding the GC somas. On the contrary, the number of these boutons was reduced to a lesser degree in the adjacent SZ and no difference was detected in the ML. We also noted a selective decrease of somatic immunoreactivity of the vesicular GABA transporter, VGAT, albeit in this case the effect was not as pronounced (Figures 3B–C and S3A–B). In addition, mice carrying TeNT had ~35% fewer neurons with detectable PV throughout the DG along with a >2-fold reduction of PV-positive puncta in the GCL, where axons of basket cells branch around the cell bodies of GCs. Yet, the processes of CR neurons terminating in the SZ were preserved (Figure 3D–G).

One disadvantage of these readouts is that the levels of GAD67 and PV are regulated by network activity (Chattopadhyaya et al., 2007; Donato et al., 2013), and depletion of antigens in otherwise intact interneurons may mimic synapse and cell loss. To bypass this problem, we tagged GCs *in vivo* with a reporter of inhibitory postsynaptic sites, gephyrin-GFP (Chen et al., 2012; van Versendaal et al., 2012) (Figure 3H). Newborn CamKIIα:Cre/R26$^{floxstop\text{-}TeNT}$ mutants were injected with AAVDJ DIO-Gephyrin-GFP to achieve sparse Cre-inducible expression of the reporter in ~10% of GCs and then analyzed by confocal imaging at P14. This technique allowed for quantification of synapses on discrete subcellular domains of single neurons. Mice with impaired vesicular release of glutamate had ~40% less gephyrin-GFP clusters on GC somas but not on proximal and distal dendrites (Figure 3I–J). A similar deficit of somatic inhibitory terminals in the GCL was revealed by electron microscopy. Interestingly, in-depth analysis of the remaining synapses showed no significant changes in their volumes, the lengths of presynaptic active zones, and the sizes of neurotransmitter vesicle pools (Figures 3K–L and S3C).

Synaptic excitation controls axon branching of Lhx6-positive interneurons

Our findings are reminiscent of recent reports that basket cells undergo structural plasticity in the CA1 and CA3 during sensory experience and memory acquisition/retrieval (Bloodgood et al., 2013; Donato et al., 2013). To explore the possibility that loss of inhibitory synapses from GC somas is attributed to abnormal morphologies of interneuron axons, we generated mice harboring CamKIIα:Cre, R26$^{floxstop\text{-}TeNT}$, and Lhx6:GFP alleles (Figure 4A). Lhx6:GFP tags GABAergic neurons that originate from the medial ganglionic eminence (MGE), including PV and SST cells populating the DG (Flandin et al., 2011;

Gittis et al., 2010) (Figure 4B). This strategy was chosen because available genetic tools were unsuitable for blocking vesicular release of glutamate and tagging basket cells in the same mice. We also took into account that down-regulation of excitatory neurotransmission had no effect on numbers of GABAergic terminals on distal segments of GC dendrites (Figures 3C and 3J), which implies that synapses of SST neurons were structurally intact.

P14 Lhx6:GFP/CamKIIα:Cre/R26$^{floxstop\text{-}TeNT}$ mutants had no apparent abnormalities in survival of MGE-derived interneurons and their distribution in the cortical columns and hippocampus (Figure 4C–E). The latter is not surprising since the onset of TeNT expression took place when interneuron migration is nearly complete (Tricoire et al., 2011). Strikingly, high resolution imaging of the DG demonstrated that glutamatergic neurotransmission profoundly affects the branching of interneuron axons. In control animals, Lhx6:GFP-positive cells established dense axonal networks near the GCs somas and their dendritic fields. The arborization was abolished in mice carrying TeNT in excitatory neurons, as evidenced by a >4-fold decrease of fine axon puncta labeled with GFP in the GCL/SZ (Figure 4F–G). Although the overlap between abundant fluorescent axons and dendrites precluded the comprehensive assessment of dendrite morphologies, we found no difference in the length of major dendritic trees and segments (data not shown).

Axonal networks of Lhx6-positive interneurons in the DG are regulated by cortical activity

To gain insight into the origin of signals that govern interneuron connectivity in the DG, we manipulated vesicular exocytosis in a region- and cell-type specific manner. In these experiments, tdTomato and TeNT were induced in brains of newborn Ai9/R26$^{floxstop\text{-}TeNT}$ mice with an AAV that encodes Cre recombinase driven by the Synapsin promoter (AAV2.2 Syn:Cre) (Figure 5A). Pups were first injected with AAV2.2 Syn:Cre into the cerebral lateral ventricles to selectively tag and silence GCs. The targeting specificity was confirmed by imaging; ~20% of mature neurons were transduced (Figures 5B–C and S4). GCs with activated Ai9 and TeNT alleles possessed normal dendritic trees, maintained axons in the CA3 and hilus for >3 weeks after the onset of recombination, and recruited SPO to their LMTs lacking Syb2 (Figure 5D–E and Table S2). In Ai9/R26$^{floxstop\text{-}TeNT}$ and control Ai9 mice, the LMTs of Cre-recombined GCs increased in size with virtually identical time-course and had comparable densities per axon length, supporting our earlier conclusion that weakened mossy fibers do not become eliminated (Figure 5F–G). Moreover, whole-cell recordings from tdTomato-positive cells showed no significant differences in sIPSC frequencies and eIPSC amplitudes, suggesting that inhibitory drive to pre-synaptically inactive GCs was unaffected (Figures 5H–I).

We then injected AAV2.2 Syn:Cre into the EC to abolish cortical excitation of the DG (Figure 6A–B). Under these conditions, recombination occurred in pyramidal neurons in the medial and lateral EC. Quantifications of boutons that recruit Syb2 confirmed that the SNARE was cleaved by TeNT in terminals of cortical axons projecting to the ML (Figures 6C–G and S5). Remarkably, inactivation of entorhinal inputs to the DG recapitulated the consequences of excitatory synapse silencing in the entire forebrain. Recordings of spontaneous and correlated IPSCs showed that P14 EC-injected Ai9/R26$^{floxstop\text{-}TeNT}$ mice had diminished inhibition of GCs (Figure 6H–I). This was not due to lower probability of

presynaptic GABA release, as the paired pulse ratios of eIPSCs elicited by stimulation of the GCL at 5–10 Hz remained the same (Figure 6J–K). By contrast, the PV immunoreactivity was reduced in the GCL by ~30% (Figure 6L–M). Lastly, targeted expression of TeNT in the EC of Lhx6:GFP/Ai9/R26$^{floxstop\text{-}TeNT}$ mutants resulted in a >2-fold decrease of Lhx6:GFP axon puncta in the GCL/SZ, suggesting that axon branching of MGE-derived interneurons was abolished (Figure 6N–O). We also noted a slight reduction in the numbers of spines on GC dendrites, which agrees with the report that vesicular release from pyramidal EC neurons stabilizes their axons (Figure S5E) (Yasuda et al., 2011).

To test how cortical activity influences the morphologies of interneuron axons in the adult DG, we injected Lhx6:GFP/Ai9/R26$^{floxstop\text{-}TeNT}$ mice with AAV2.2 Syn:Cre into one hemisphere at P60 (Figure 6P). The GFP-tagged cells were inspected two weeks later in the target ipsilateral side of the DG and in the contralateral side that receives intact afferents. Again, induction of TeNT in the EC interfered with axon branching, whereas injection of the virus into the brains of control Ai9/Lhx6:GFP mice had no effect (Figure 6Q–R).

Analysis of GC inhibition in mice deficient for NMDA receptors in PV neurons and GCs

Similar to GCs, basket cells in the DG are innervated by projection EC neurons and generate NMDA- and AMPA-type currents in response to cortical excitation (Sambandan et al., 2010; Zipp et al., 1989). Intriguingly, global ablation of NMDA receptors in PV cells impaired hippocampal synchronicity, spatial representations, and memory (Carlen et al., 2012; Korotkova et al., 2010), but the extent to which these behavioral abnormalities are linked with reorganization of connectivity was unknown. One interpretation of our findings is that axonal networks of basket cells are regulated by direct glutamatergic inputs onto these interneurons. However, it is conceivable that formation of GABAergic terminals on GC somas depends on activity of GCs. In such a case, changes in axon branching may be mediated by retrograde signals or merely reflect pruning that follows synapse loss. Given these scenarios and a limited precision of Lhx6:GFP tracing, we examined mice that lacked NMDA receptors in either PV cells or GCs.

Our laboratory recently designed a new form of inducible Cre (DD-Cre) whose stability and capacity to catalyze loxP recombination is acutely regulated by the antibiotic, Trimethoprim (TMP). TMP efficiently crosses the blood-brain barrier and, by binding to DD-Cre, mediates rapid excision of “floxed” sequences on genomic and episomal viral DNA (Sando et al., 2013). We took advantage of this method to produce conditional knock-out (cKO) of NMDA receptors in PV cells with the developmental time-course which is similar to manipulations of vesicular release with TeNT. For this purpose, we utilized a knock-in allele that drives DD-Cre under the control of the Pvalb promoter (Pvalb:2A-DD-Cre). In these line, a cassette encoding the T2A self-cleaving peptide fused with DD-Cre was inserted at the end of the last exon of the Pvalb gene to preserve the expression of endogenous PV (Harris et al., 2014). Pvalb:2A-DD-Cre mice had no constitutive recombination in the cortex and hippocampus, as assessed with the Ai9 reporter. Intra-peritoneal (i.p.) injections of TMP induced recombination exclusively in cells that were positive for PV and fired action potentials at high frequency during depolarization (Figure S6).

We then crossed Ai9/Pvalb:2A-DD-Cre mice with an allele that harbors *loxP* sites flanking several exons of Grin1 (Grin1$^{flox/flox}$), a gene encoding the NMDA receptor NR1 subunit that forms the ion channel pore (McHugh et al., 2007) (Figure 7A). It has been shown that NMDA-type currents become suppressed ~2 weeks after Grin1 deletion, most likely due to slow decay of pre-existing mRNA and protein (Adesnik et al., 2008). We therefore treated mice with 3 sequential TMP doses stating at P9 and examined them at P25. This protocol yielded recombination in >90% of PV cells in the DG. Whole-cell recordings from tdTomato-tagged interneurons confirmed a strong down-regulation of NMDA-type currents with no effect on AMPA-type eEPSCs (Figures 7B–C and S6C).

Having established this chemical-genetic system, we asked how cKO of NMDA receptors in PV cells affects the GABAergic inhibition in the DG. To this end, whole-cell recordings of spontaneous and correlated IPSCs were carried out from reporter-negative GCs. TMP-treated Pvalb:2A-DD-Cre/Ai9/Grin1$^{flox/flox}$ mice had a ~30–40% decrease in sIPSC frequencies and eIPSC amplitudes. In contrast, these animals and their Grin1$^{flox/flox}$ littermates had indistinguishable sizes of sIPSCs and eIPSC paired pulse ratios, indirectly suggesting that reduced strength of GABAergic inputs to GCs was due to loss of innervation by interneurons (Figures 7D–E and S7).

In complementary experiments, Grin1 was selectively knocked out in GCs (Figure 7F). This was achieved by injecting Ai9/Grin1$^{flox/flox}$ mice with AAV2.2 Syn:Cre into the cerebral lateral ventricles, as described above. Again, electrophysiology confirmed the suppression of NMDA but not AMPA currents in reporter-positive neurons. However, analyses of IPSCs demonstrated that the spontaneous and correlated inhibition of Grin1-deficient GCs was normal (Figures 7G–J). To further examine inhibitory synapses by confocal imaging, we co-injected animals with AAV2.2 Syn:Cre and AAV2.2 DIO-Gephyrin-GFP. No difference in the abundance of gephyrin-GFP clusters was observed across all subcellular domains of Grin1 cKO neurons (Figure S8). Hence, NMDA receptor activity in GCs appears to be dispensable for regulation of their inhibition.

NMDA receptors regulate the morphologies of interneuron axons

The evidence thus far supports the model that glutamatergic inputs onto PV neurons modulate their outputs to GCs in an NMDA receptor-dependent manner. To directly test if this phenomenon involves rearrangement of interneuron connectivity, we interrogated the structures of isolated Grin1-deficient PV cells that were tagged *in vivo* with two fluorescent reporters (Figure 8A). Newborn Pvalb:2A-DD-Cre/Ai9/Grin1$^{flox/flox}$ mice were injected with an AAV that encodes a Cre-inducible version of pre-synaptic marker, synaptophysin-GFP (O'Sullivan et al., 2014) (AAVDJ DIO-SyP-GFP). These animals were then treated with TMP at P9, and analyzed by confocal imaging of brain sections at P25. To minimize the overlap of fluorescent processes that belong to neighboring neurons, recombination was induced in a sparse manner with one TMP pulse. tdTomato and synaptophysin-GFP were expressed in ~30% of PV cells in the DG, resulting in bright dual-color labeling of their dendrites, axons and pre-synaptic terminals (Figure 8B). We acquired 3D image stacks and counted axonal/presynaptic puncta that were positive for both reporters to avoid contamination with tdTomato signal from adjacent dendrites. These measurements

demonstrated that Pvalb:2A-DD-Cre/Ai9/Grin1$^{flox/flox}$ mutants had a ~2-fold reduction in the total puncta density in the GCL with no changes in sizes of individual boutons and their linear densities along each axon segment (Figure 8C–D). Furthermore, quantitative analysis of reconstructed dendrites showed no abnormalities in their length and complexities (Figure 8E–F). These results indicate that loss of NMDA receptors does not impair the differentiation of PV cell dendrites and synaptogenic potential of single axon arbors. Rather, activity-dependent control of synaptic networks likely occurs at a level of axon branching, which ultimately dictates the pattern of GC innervation by each interneuron.

DISCUSSION

In summary, these experiments provide new insights into how excitatory neurotransmission impacts the connectivity in the DG.

Contribution of activity to presynaptic differentiation of GCs

Vesicular exocytosis is known to be essential for the development of glutamatergic axons and synapses in many circuits. For example, targeted expression of TeNT impaired the wiring of olfactory sensory neurons, photoreceptors, and projection pyramidal neurons in the somatosensory cortex (Kerschensteiner et al., 2009; Wang et al., 2007; Yu et al., 2004). It is quite striking that, in our hands, a similar approach revealed no detectable consequences of presynaptic silencing on patterning of GC mossy fibers and LMTs. Because Syb2 is required for action potential-driven and spontaneous vesicle fusion alike (Maximov et al., 2009; Schoch et al., 2001), neither modality of release appears to be necessary for mossy fiber differentiation. Our results are at odds with the recent study proposing that synaptic outputs from the DG to the CA3 are refined through competition between axons of mature and young GCs, and that mossy fibers of neurons carrying TeNT become eliminated (Yasuda et al., 2011). It is possible that this discrepancy is attributed to differences in timing of TeNT induction and expression levels of the protease. Nevertheless, activity-dependent competition is irreconcilable with the large body of work that describes the physiological properties of GCs and their relevance to memory acquisition/recall. LMTs have relatively low probability of neurotransmitter release, and only a small fraction of GCs is active in any environment due to sparse coding of information incoming from the cortex (Leutgeb et al., 2007; Nicoll and Schmitz, 2005; Treves et al., 2008). Extinction of “silent” terminals might dampen transiently activated neurons from a network, however, associative memories could be retrieved by optogenetic stimulation of GCs tagged during learning (Liu et al., 2012). Lastly, projections of GCs expressing TeNT from an inducible promoter have been shown to be intact in the adult brain (Lopez et al., 2012). It is essential to note that experience may alter GCs presynaptically through Hebbian plasticity, remodeling of filopodial synapses, and rapid LMT turnover (Castillo et al., 2002; Galimberti et al., 2010; Ruediger et al., 2011). In spite of that, the axons of these neurons are likely “hard-wired”.

Excitatory neurotransmission and presynaptic networks of dentate interneurons

A critical role of experience in regulating the connectivity of GABAergic neurons has been appreciated in the cerebral cortex, CA1 and CA3 (Bloodgood et al., 2013; Chattopadhyaya et al., 2007; Chen et al., 2012; Donato et al., 2013; Keck et al., 2011; van Versendaal et al.,

2012). Furthermore, electrophysiological studies in the olfactory, auditory and somatosensory cortex suggested that inhibition is commonly proportional to excitation (Poo and Isaacson, 2009; Wehr and Zador, 2003; Wilent and Contreras, 2005; Zhang et al., 2003). Evidently, a similar balance is maintained in the developing DG via redistribution of GABAergic synapses formed on GC somas by PV basket cells. While our initial observations are not entirely unexpected, we ultimately identify new principles of basket cell plasticity that operate in this and, perhaps, other circuits.

First, we demonstrate that networks of PV cells in the DG are strongly influenced by release from projection EC neurons and by NMDA receptors in interneurons. At the same time, neither presynaptic silencing of GCs nor knockout of their NMDA receptors had apparent effects on GC inhibition. Taken together, these results support the model that dentate PV cells are capable of adjusting the patterns of somatic innervation depending on the strength of direct cortical excitation rather than glutamatergic inputs and/or retrograde signals from local reciprocally connected GCs. Another important aspect of experiments with TMP-inducible Grin1 cKO mice, is that they validate the specificity of phenotypes associated with expression of TeNT in the EC. Aside from blocking the release of glutamate, cleavage of vesicular SNAREs in pyramidal neurons may interfere with secretion of diffusible proteins such as BDNF (Matsuda et al., 2009) and our unpublished work). While the involvement of these cues in structural remodeling of dentate interneurons cannot be completely ruled out, fast neurotransmission clearly plays a major part.

Second, we provide evidence that activity-dependent changes in PV neuron connectivity are largely axon-specific. Indeed, loss of GC innervation does not coincide with abnormalities in the ultra-structural organization of somatic GABAergic terminals and their linear density per axon branch, as assessed in CamKIIα:Cre/R26$^{floxstop\text{-}TeNT}$ and Pvalb:2A-DD-Cre/Ai9/Grin1$^{flox/flox}$ mice, respectively. Moreover, NMDA receptor-deficient interneurons have normal dendrites. Thus, expansion/retraction of basket cell axons is likely the primary driving force for rewiring. Given the involvement of PV neurons and their NMDA receptors in gamma-oscillations, spatial representations and memory (Carlen et al., 2012; Korotkova et al., 2010; Sohal et al., 2009), this powerful mechanism may be essential for a variety of cortical and hippocampal-dependent tasks.

Considering the slow time-course of synaptic silencing in our mouse models, the temporal dynamics of basket cell rewiring need to be further defined. In addition, it will be of great interest to identify the downstream substrates of NMDA receptors in these interneurons. In the CA1, experience-dependent rearrangement of somatic inhibitory terminals is orchestrated by activity-induced transcription factor, Npas4, in pyramidal cells (Bloodgood et al., 2013). Intriguingly, Npas4 also regulates gene expression in MGE-derived interneurons, making it an attractive candidate for basket cell plasticity (Spiegel et al., 2014). Besides Npas4, NMDA receptors may influence the presynaptic differentiation of PV neurons through activity-dependent synthesis of GABA or LKB1-NUAK1 kinase pathway that has been implicated in axon branching of pyramidal cortical neurons (Chattopadhyaya et al., 2007; Courchet et al., 2013). On a technical note, we must acknowledge that Pvalb promoter is also on in chandelier cells that innervate axons (Taniguchi et al., 2013), but our readouts do not account for possible effects of activity on axonal inhibition of GCs. Finally,

it remains unclear whether GCs and dentate basket cells receive excitatory inputs from the same population of EC neurons. Addressing these questions will be necessary for further understanding interneuron plasticity and information coding in the DG.

EXPERIMENTAL PROCEDURES

Mice

The Ai9, CamKIIα:Cre, R26$^{floxstop\text{-}TeNT}$, Lhx6:GFP and Grin1$^{flox/flox}$ alleles were previously characterized (Gittis et al., 2010; Madisen et al., 2010; McHugh et al., 2007; Saura et al., 2004; Zhang et al., 2008). To generate the Pvalb:2A-DD-Cre driver line, a cassette encoding the T2A self-cleaving peptide followed by the published DD-Cre sequence (Sando et al., 2013) was inserted via homologous recombination in the 3′-UTR of the Pvalb gene immediately after the last exon (Harris et al., 2014). Mice were housed and analyzed according to protocols approved by the IACUC committee.

Virus design and injection

AAVs were produced with a shuttle vector containing inverted terminal repeats, the WPRE element and the hGH polyadenylation signal (Cardin et al., 2010). For Cre-inducible expression of mGFP, gephyrin-GFP and synaptophysin-GFP, coding sequences were flanked by two pairs of loxP sites (DIO) and inserted downstream of a 1.26 kb EF1α promoter in a 3′–5′ orientation. Sequence encoding Cre recombinase was subcloned downstream of a 1.1 kb rat Synapsin promoter in a 5′–3′ orientation. Pups were anesthetized on ice and injected with 0.5μl of the viral stock using a glass micropipette (10μm tip).

TMP-inducible recombination

TMP lactate was reconstituted in water at a concentration of 200 mg/ml; this stock was then diluted in PBS. Intra-peritoneal (i.p.) injections were performed as described (Sando et al., 2013) to deliver TMP doses of 0.3 mg/gm body weight/day. Vehicle solution contained PBS alone.

Immunohistochemistry

Mice were anesthetized with isofluorane and perfused with ice cold solution containing 4% PFA. The brains were incubated overnight in 0.5% PFA, and sliced in PBS using a vibratome. The 90μm thick brain sections were blocked in 4% BSA, 2% horse serum and 0.2% Triton. Sections were then incubated with primary antibodies and fluorescently labeled secondary antibodies, washed, and mounted for analysis.

Confocal imaging

Images were collected under the Nikon C2 microscope with 10/20x dry objectives and 40/60x oil immersion objectives. Digital images were acquired with Nikon Elements and analyzed with Volocity and Neurolucida software. The numbers of synaptic and axon puncta were automatically counted in 3D stack volumes after uniform thresholding. Data were normalized to control animals for each littermate pair and then averaged.

Electron microscopy

Animals were perfused with 100 mM Na-cacodylate, 2% PFA, 2.5% glutaraldehyde and 1% sucrose. 100 μm Vibratome sections were incubated in 1% OsO_4, 1.5% potassium hexacyanoferrate in 0.1 M cacodylate buffer, and then dehydrated with ethanol. Subsequently, sections were contrasted in 2% uranyl acetate, washed and embedded in Epon. Samples were counterstained with lead citrate and examined under the Philips CM 100 electron microscope.

Electrophysiology

Acute slices were bathed in oxygenized artificial cerebrospinal fluid. Whole-cell recordings were performed at room temperature using a Multiclamp 700B amplifier. Extracellular stimuli were controlled with Model 2100 Isolated Pulse Stimulator. Currents were sampled at 10 kHz and analyzed offline using pClamp10 and Origin8 software.

Statistical analyses were performed using Student's t-test (two-tailed distribution). All quantifications are represented as Mean±S.E.M. * denote $P<0.05$.

Supplementary Material

Refer to Web version on PubMed Central for supplementary material.

Acknowledgments

We thank Drs. Hollis Cline, Franck Polleux and Kiriana Cowansage for advice and critical comments; Drs. Thomas Südhof, Martyn Goulding and Ulrich Müller for providing mouse strains and antibodies; members of the TSRI DNC for help with experiments; and Dr. Kathy Spencer and the Salk Viral Vector core for technical assistance. This study was supported by the NIH grants MH085776 (A.M.), NS087026 (A.M.) and EY016807 (S. Panda), Novartis ADI (A.M.), The Baxter Foundation (A.M.), and Helen Dorris Postdoctoral Fellowship (S. Pieraut.)

References

Acsady L, Kali S. Models, structure, function: the transformation of cortical signals in the dentate gyrus. Progress in brain research. 2007; 163:577–599. [PubMed: 17765739]

Adesnik H, Li G, During MJ, Pleasure SJ, Nicoll RA. NMDA receptors inhibit synapse unsilencing during brain development. Proceedings of the National Academy of Sciences of the United States of America. 2008; 105:5597–5602. [PubMed: 18375768]

Bagnall MW, Hull C, Bushong EA, Ellisman MH, Scanziani M. Multiple clusters of release sites formed by individual thalamic afferents onto cortical interneurons ensure reliable transmission. Neuron. 2011; 71:180–194. [PubMed: 21745647]

Basu J, Srinivas KV, Cheung SK, Taniguchi H, Huang ZJ, Siegelbaum SA. A cortico-hippocampal learning rule shapes inhibitory microcircuit activity to enhance hippocampal information flow. Neuron. 2013; 79:1208–1221. [PubMed: 24050406]

Bloodgood BL, Sharma N, Browne HA, Trepman AZ, Greenberg ME. The activity-dependent transcription factor NPAS4 regulates domain-specific inhibition. Nature. 2013; 503:121–125. [PubMed: 24201284]

Bortone D, Polleux F. KCC2 expression promotes the termination of cortical interneuron migration in a voltage-sensitive calcium-dependent manner. Neuron. 2009; 62:53–71. [PubMed: 19376067]

Burger C, Gorbatyuk OS, Velardo MJ, Peden CS, Williams P, Zolotukhin S, Reier PJ, Mandel RJ, Muzyczka N. Recombinant AAV viral vectors pseudotyped with viral capsids from serotypes 1, 2, and 5 display differential efficiency and cell tropism after delivery to different regions of the central

nervous system. Molecular therapy: the journal of the American Society of Gene Therapy. 2004; 10:302–317. [PubMed: 15294177]

Cardin JA, Carlen M, Meletis K, Knoblich U, Zhang F, Deisseroth K, Tsai LH, Moore CI. Targeted optogenetic stimulation and recording of neurons in vivo using cell-type-specific expression of Channelrhodopsin-2. Nature protocols. 2010; 5:247–254.

Carlen M, Meletis K, Siegle JH, Cardin JA, Futai K, Vierling-Claassen D, Ruhlmann C, Jones SR, Deisseroth K, Sheng M, et al. A critical role for NMDA receptors in parvalbumin interneurons for gamma rhythm induction and behavior. Molecular psychiatry. 2012; 17:537–548. [PubMed: 21468034]

Castillo PE, Schoch S, Schmitz F, Sudhof TC, Malenka RC. RIM1alpha is required for presynaptic long-term potentiation. Nature. 2002; 415:327–330. [PubMed: 11797010]

Chattopadhyaya B, Di Cristo G, Higashiyama H, Knott GW, Kuhlman SJ, Welker E, Huang ZJ. Experience and activity-dependent maturation of perisomatic GABAergic innervation in primary visual cortex during a postnatal critical period. The Journal of neuroscience: the official journal of the Society for Neuroscience. 2004; 24:9598–9611. [PubMed: 15509747]

Chattopadhyaya B, Di Cristo G, Wu CZ, Knott G, Kuhlman S, Fu Y, Palmiter RD, Huang ZJ. GAD67-mediated GABA synthesis and signaling regulate inhibitory synaptic innervation in the visual cortex. Neuron. 2007; 54:889–903. [PubMed: 17582330]

Chen JL, Lin WC, Cha JW, So PT, Kubota Y, Nedivi E. Structural basis for the role of inhibition in facilitating adult brain plasticity. Nature neuroscience. 2011; 14:587–594.

Chen JL, Villa KL, Cha JW, So PT, Kubota Y, Nedivi E. Clustered dynamics of inhibitory synapses and dendritic spines in the adult neocortex. Neuron. 2012; 74:361–373. [PubMed: 22542188]

Courchet J, Lewis TL Jr, Lee S, Courchet V, Liou DY, Aizawa S, Polleux F. Terminal axon branching is regulated by the LKB1-NUAK1 kinase pathway via presynaptic mitochondrial capture. Cell. 2013; 153:1510–1525. [PubMed: 23791179]

De Marco Garcia NV, Karayannis T, Fishell G. Neuronal activity is required for the development of specific cortical interneuron subtypes. Nature. 2011; 472:351–355. [PubMed: 21460837]

DeFelipe J, Lopez-Cruz PL, Benavides-Piccione R, Bielza C, Larranaga P, Anderson S, Burkhalter A, Cauli B, Fairen A, Feldmeyer D, et al. New insights into the classification and nomenclature of cortical GABAergic interneurons. Nature reviews Neuroscience. 2013; 14:202–216.

Donato F, Rompani SB, Caroni P. Parvalbumin-expressing basket-cell network plasticity induced by experience regulates adult learning. Nature. 2013; 504:272–276. [PubMed: 24336286]

Fishell G, Rudy B. Mechanisms of inhibition within the telencephalon: “where the wild things are”. Annual review of neuroscience. 2011; 34:535–567.

Flandin P, Zhao Y, Vogt D, Jeong J, Long J, Potter G, Westphal H, Rubenstein JL. Lhx6 and Lhx8 coordinately induce neuronal expression of Shh that controls the generation of interneuron progenitors. Neuron. 2011; 70:939–950. [PubMed: 21658586]

Forster E, Zhao S, Frotscher M. Laminating the hippocampus. Nature reviews Neuroscience. 2006; 7:259–267.

Galimberti I, Bednarek E, Donato F, Caroni P. EphA4 signaling in juveniles establishes topographic specificity of structural plasticity in the hippocampus. Neuron. 2010; 65:627–642. [PubMed: 20223199]

Gittis AH, Nelson AB, Thwin MT, Palop JJ, Kreitzer AC. Distinct roles of GABAergic interneurons in the regulation of striatal output pathways. The Journal of neuroscience: the official journal of the Society for Neuroscience. 2010; 30:2223–2234. [PubMed: 20147549]

Harris JA, Hirokawa KE, Sorensen SA, Gu H, Mills M, Ng LL, Bohn P, Mortrud M, Ouellette B, Kidney J, et al. Anatomical characterization of Cre driver mice for neural circuit mapping and manipulation. Frontiers in neural circuits. 2014; 8:76. [PubMed: 25071457]

Hosp JA, Struber M, Yanagawa Y, Obata K, Vida I, Jonas P, Bartos M. Morpho-physiological criteria divide dentate gyrus interneurons into classes. Hippocampus. 2014; 24:189–203. [PubMed: 24108530]

Houser CR. Interneurons of the dentate gyrus: an overview of cell types, terminal fields and neurochemical identity. Progress in brain research. 2007; 163:217–232. [PubMed: 17765721]

Isaacson JS, Scanziani M. How inhibition shapes cortical activity. Neuron. 2011; 72:231–243. [PubMed: 22017986]

Keck T, Scheuss V, Jacobsen RI, Wierenga CJ, Eysel UT, Bonhoeffer T, Hubener M. Loss of sensory input causes rapid structural changes of inhibitory neurons in adult mouse visual cortex. Neuron. 2011; 71:869–882. [PubMed: 21903080]

Kerschensteiner D, Morgan JL, Parker ED, Lewis RM, Wong RO. Neurotransmission selectively regulates synapse formation in parallel circuits in vivo. Nature. 2009; 460:1016–1020. [PubMed: 19693082]

Korotkova T, Fuchs EC, Ponomarenko A, von Engelhardt J, Monyer H. NMDA receptor ablation on parvalbumin-positive interneurons impairs hippocampal synchrony, spatial representations, and working memory. Neuron. 2010; 68:557–569. [PubMed: 21040854]

Kullmann DM, Moreau AW, Bakiri Y, Nicholson E. Plasticity of inhibition. Neuron. 2012; 75:951–962. [PubMed: 22998865]

Leutgeb JK, Leutgeb S, Moser MB, Moser EI. Pattern separation in the dentate gyrus and CA3 of the hippocampus. Science. 2007; 315:961–966. [PubMed: 17303747]

Lin Y, Bloodgood BL, Hauser JL, Lapan AD, Koon AC, Kim TK, Hu LS, Malik AN, Greenberg ME. Activity-dependent regulation of inhibitory synapse development by Npas4. Nature. 2008; 455:1198–1204. [PubMed: 18815592]

Liu X, Ramirez S, Pang PT, Puryear CB, Govindarajan A, Deisseroth K, Tonegawa S. Optogenetic stimulation of a hippocampal engram activates fear memory recall. Nature. 2012; 484:381–385. [PubMed: 22441246]

Lopez CM, Pelkey KA, Chittajallu R, Nakashiba T, Toth K, Tonegawa S, McBain CJ. Competition from newborn granule cells does not drive axonal retraction of silenced old granule cells in the adult hippocampus. Frontiers in neural circuits. 2012; 6:85. [PubMed: 23162435]

Madisen L, Zwingman TA, Sunkin SM, Oh SW, Zariwala HA, Gu H, Ng LL, Palmiter RD, Hawrylycz MJ, Jones AR, et al. A robust and high-throughput Cre reporting and characterization system for the whole mouse brain. Nature neuroscience. 2010; 13:133–140.

Maffei A, Nelson SB, Turrigiano GG. Selective reconfiguration of layer 4 visual cortical circuitry by visual deprivation. Nature neuroscience. 2004; 7:1353–1359.

Matsuda N, Lu H, Fukata Y, Noritake J, Gao H, Mukherjee S, Nemoto T, Fukata M, Poo MM. Differential activity-dependent secretion of brain-derived neurotrophic factor from axon and dendrite. The Journal of neuroscience: the official journal of the Society for Neuroscience. 2009; 29:14185–14198. [PubMed: 19906967]

Maximov A, Tang J, Yang X, Pang ZP, Sudhof TC. Complexin controls the force transfer from SNARE complexes to membranes in fusion. Science. 2009; 323:516–521. [PubMed: 19164751]

McHugh TJ, Jones MW, Quinn JJ, Balthasar N, Coppari R, Elmquist JK, Lowell BB, Fanselow MS, Wilson MA, Tonegawa S. Dentate gyrus NMDA receptors mediate rapid pattern separation in the hippocampal network. Science. 2007; 317:94–99. [PubMed: 17556551]

Nakashiba T, Cushman JD, Pelkey KA, Renaudineau S, Buhl DL, McHugh TJ, Rodriguez Barrera V, Chittajallu R, Iwamoto KS, McBain CJ, et al. Young dentate granule cells mediate pattern separation, whereas old granule cells facilitate pattern completion. Cell. 2012; 149:188–201. [PubMed: 22365813]

Nicoll RA, Schmitz D. Synaptic plasticity at hippocampal mossy fibre synapses. Nature reviews Neuroscience. 2005; 6:863–876.

O'Sullivan ML, Martini F, von Daake S, Comoletti D, Ghosh A. LPHN3, a presynaptic adhesion-GPCR implicated in ADHD, regulates the strength of neocortical layer 2/3 synaptic input to layer 5. Neural development. 2014; 9:7. [PubMed: 24739570]

Poo C, Isaacson JS. Odor representations in olfactory cortex: "sparse" coding, global inhibition, and oscillations. Neuron. 2009; 62:850–861. [PubMed: 19555653]

Ruediger S, Vittori C, Bednarek E, Genoud C, Strata P, Sacchetti B, Caroni P. Learning-related feedforward inhibitory connectivity growth required for memory precision. Nature. 2011; 473:514–518. [PubMed: 21532590]

Sambandan S, Sauer JF, Vida I, Bartos M. Associative plasticity at excitatory synapses facilitates recruitment of fast-spiking interneurons in the dentate gyrus. The Journal of neuroscience: the official journal of the Society for Neuroscience. 2010; 30:11826–11837. [PubMed: 20810902]

Sando R 3rd, Baumgaertel K, Pieraut S, Torabi-Rander N, Wandless TJ, Mayford M, Maximov A. Inducible control of gene expression with destabilized Cre. Nature methods. 2013; 10:1085–1088. [PubMed: 24056874]

Sando R 3rd, Gounko N, Pieraut S, Liao L, Yates J 3rd, Maximov A. HDAC4 governs a transcriptional program essential for synaptic plasticity and memory. Cell. 2012; 151:821–834. [PubMed: 23141539]

Saura CA, Choi SY, Beglopoulos V, Malkani S, Zhang D, Shankaranarayana Rao BS, Chattarji S, Kelleher RJ 3rd, Kandel ER, Duff K, et al. Loss of presenilin function causes impairments of memory and synaptic plasticity followed by age-dependent neurodegeneration. Neuron. 2004; 42:23–36. [PubMed: 15066262]

Schoch S, Deak F, Konigstorfer A, Mozhayeva M, Sara Y, Sudhof TC, Kavalali ET. SNARE function analyzed in synaptobrevin/VAMP knockout mice. Science. 2001; 294:1117–1122. [PubMed: 11691998]

Sohal VS, Zhang F, Yizhar O, Deisseroth K. Parvalbumin neurons and gamma rhythms enhance cortical circuit performance. Nature. 2009; 459:698–702. [PubMed: 19396159]

Spiegel I, Mardinly AR, Gabel HW, Bazinet JE, Couch CH, Tzeng CP, Harmin DA, Greenberg ME. Npas4 Regulates Excitatory-Inhibitory Balance within Neural Circuits through Cell-Type-Specific Gene Programs. Cell. 2014; 157:1216–1229. [PubMed: 24855953]

Taniguchi H, Lu J, Huang ZJ. The spatial and temporal origin of chandelier cells in mouse neocortex. Science. 2013; 339:70–74. [PubMed: 23180771]

Treves A, Tashiro A, Witter MP, Moser EI. What is the mammalian dentate gyrus good for? Neuroscience. 2008; 154:1155–1172. [PubMed: 18554812]

Tricoire L, Pelkey KA, Erkkila BE, Jeffries BW, Yuan X, McBain CJ. A blueprint for the spatiotemporal origins of mouse hippocampal interneuron diversity. The Journal of neuroscience: the official journal of the Society for Neuroscience. 2011; 31:10948–10970. [PubMed: 21795545]

van Groen T, Miettinen P, Kadish I. The entorhinal cortex of the mouse: organization of the projection to the hippocampal formation. Hippocampus. 2003; 13:133–149. [PubMed: 12625464]

van Versendaal D, Rajendran R, Saiepour MH, Klooster J, Smit-Rigter L, Sommeijer JP, De Zeeuw CI, Hofer SB, Heimel JA, Levelt CN. Elimination of inhibitory synapses is a major component of adult ocular dominance plasticity. Neuron. 2012; 74:374–383. [PubMed: 22542189]

Wang CL, Zhang L, Zhou Y, Zhou J, Yang XJ, Duan SM, Xiong ZQ, Ding YQ. Activity-dependent development of callosal projections in the somatosensory cortex. The Journal of neuroscience: the official journal of the Society for Neuroscience. 2007; 27:11334–11342. [PubMed: 17942728]

Wehr M, Zador AM. Balanced inhibition underlies tuning and sharpens spike timing in auditory cortex. Nature. 2003; 426:442–446. [PubMed: 14647382]

Wilent WB, Contreras D. Dynamics of excitation and inhibition underlying stimulus selectivity in rat somatosensory cortex. Nature neuroscience. 2005; 8:1364–1370.

Yasuda M, Johnson-Venkatesh EM, Zhang H, Parent JM, Sutton MA, Umemori H. Multiple forms of activity-dependent competition refine hippocampal circuits in vivo. Neuron. 2011; 70:1128–1142. [PubMed: 21689599]

Yu CR, Power J, Barnea G, O'Donnell S, Brown HE, Osborne J, Axel R, Gogos JA. Spontaneous neural activity is required for the establishment and maintenance of the olfactory sensory map. Neuron. 2004; 42:553–566. [PubMed: 15157418]

Zhang LI, Tan AY, Schreiner CE, Merzenich MM. Topography and synaptic shaping of direction selectivity in primary auditory cortex. Nature. 2003; 424:201–205. [PubMed: 12853959]

Zhang Y, Narayan S, Geiman E, Lanuza GM, Velasquez T, Shanks B, Akay T, Dyck J, Pearson K, Gosgnach S, et al. V3 spinal neurons establish a robust and balanced locomotor rhythm during walking. Neuron. 2008; 60:84–96. [PubMed: 18940590]

Zipp F, Nitsch R, Soriano E, Frotscher M. Entorhinal fibers form synaptic contacts on parvalbumin-immunoreactive neurons in the rat fascia dentata. Brain research. 1989; 495:161–166. [PubMed: 2776034]

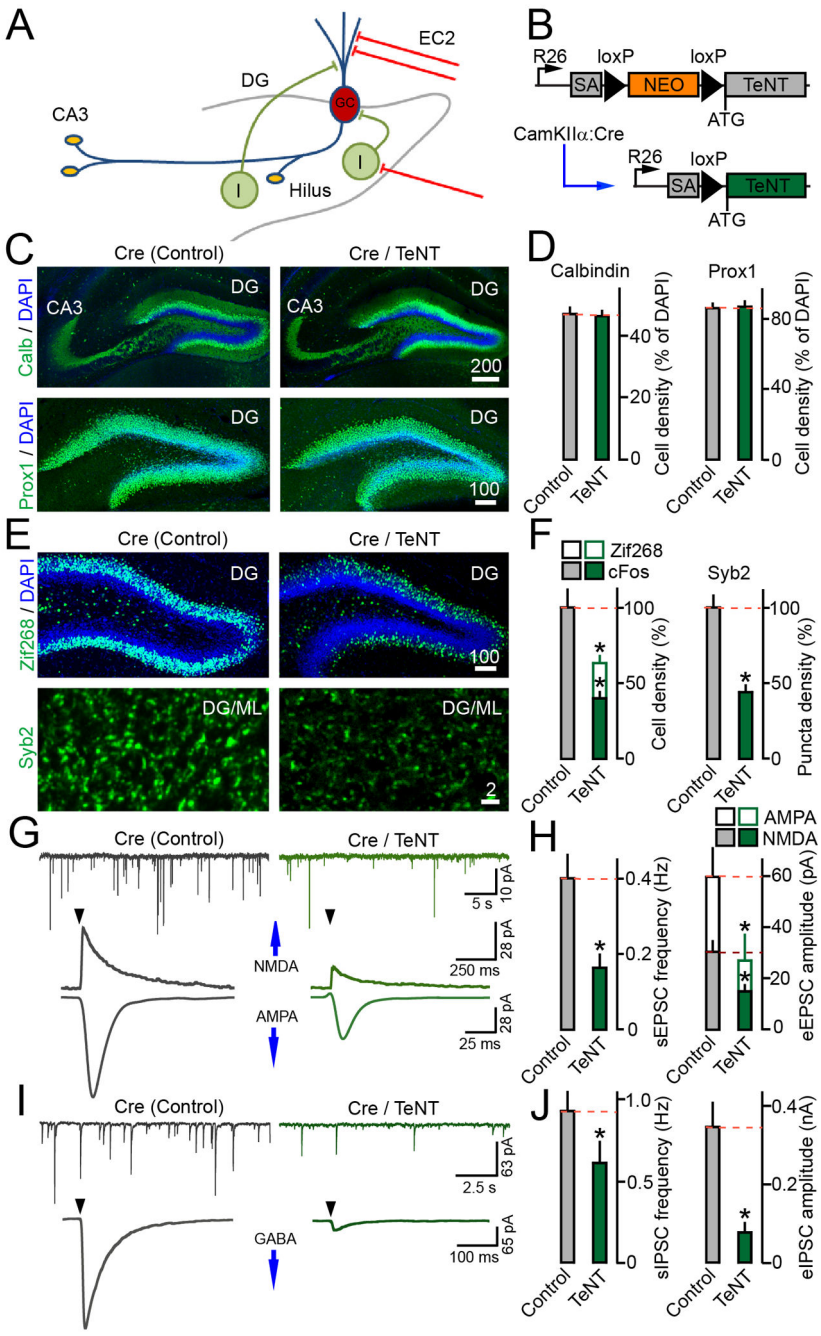

Figure 1. Relationship between synaptic excitation an inhibition of GCs

(A) Schematic representation of connectivity in the DG. GC=granule cell; I=interneuron; EC2=axons of entorhinal cortical neurons.

(B) Cre-inducible expression of tetanus toxin in CamKIIα:Cre/R26$^{\text{floxstop-TeNT}}$ mice. These mutants (Cre/TeNT) and their TeNT-negative littermates (Cre) were analyzed at P14.

(C) Images of the DG in brain sections labeled with DAPI and antibodies to GC-specific markers, calbindin and prox1. In all image frames, scale bars are shown in micrometers.

(D) Averaged densities of calbindin- and prox1-positive GCs. *N*=3 mice/genotype. Calbindin, P=0.85; prox1, P=0.9.

(E) Sections were stained with antibodies to Zif268 or Syb2. Images of the entire DG and GC dendritic fields in the ML are displayed.

(F) Densities of GCs immunoreactive for Zif268 and cFos, and Syb2-positive puncta in the ML. *N*=3 mice/genotype. Zif268, P<0.001; c-Fos, P<0.001; Syb2, P<0.001.

(G) Traces of spontaneous and evoked AMPA and NMDA-type EPSCs monitored from GCs in acute brain slices. Whole-cell recordings were performed in the presence of the GABA receptor blocker, gabazine. Evoked responses were elicited by extracellular stimulation of the perforant path at 0.1 Hz (arrows). Holding potentials (Vm) were −70mV and +40mV for AMPA and NMDA currents, respectively.

(H) Mean sEPSC frequencies and eEPSCs amplitudes. sEPSCs: Control, *N*=6 mice/20 neurons; TeNT, *N*=4 mice/12 neurons, P<0.001. eEPSCs: Control, *N*=6 mice/15 neurons; TeNT, *N*=4 mice/15 neurons, P<0.05.

(I) Samples of spontaneous and evoked IPSCs recorded from GCs in the presence of AMPA and NMDA receptor blockers, DNQX and APV. Correlated responses were triggered by stimulation of the GCL. Vm was −70mV.

(J) Mean sIPSC frequencies and eIPSC amplitudes. sIPSCs: *N*=3 mice/14–15 neurons/genotype, P<0.05. eIPSCs: *N*=3 mice/11–12 neurons/genotype, P<0.02.

See also Figure S1 and Table S1.

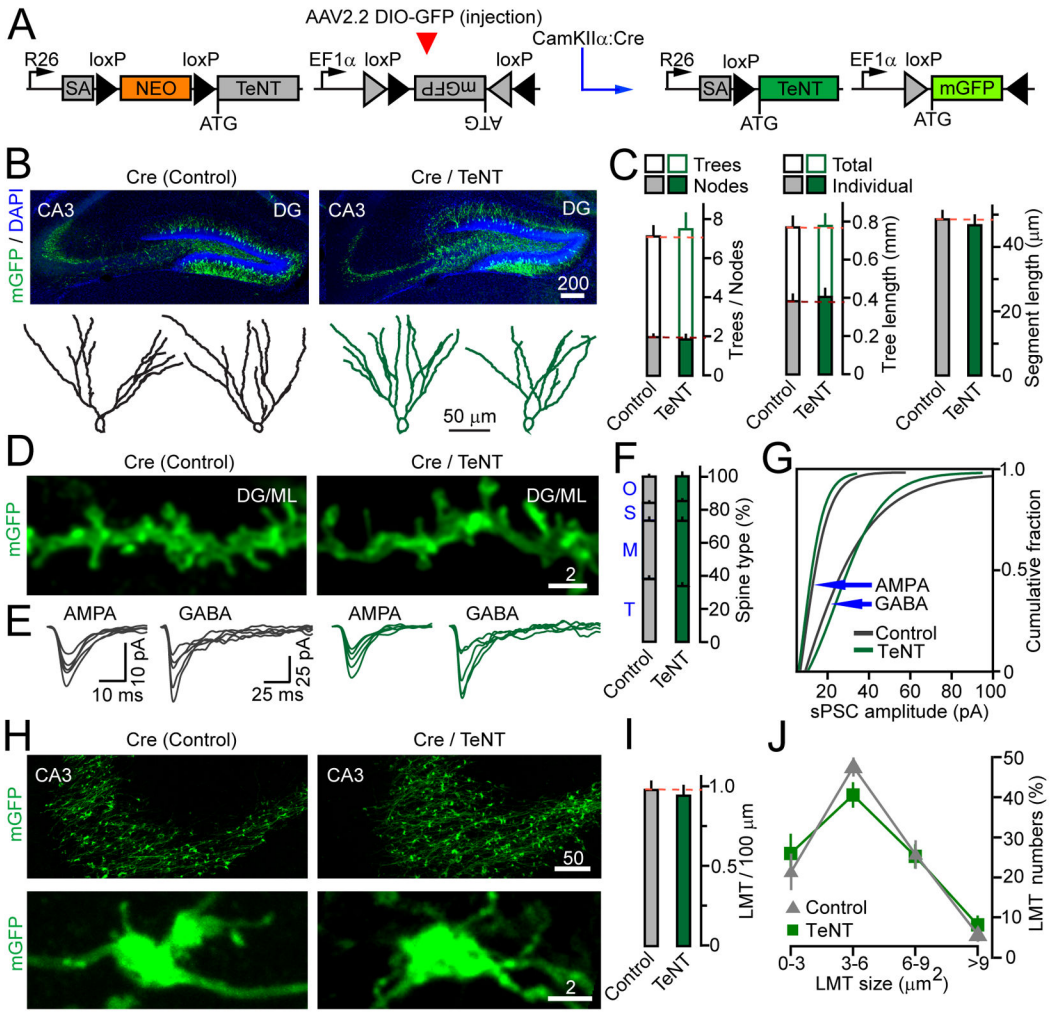

Figure 2. Analysis of GCs dendrites and axons in CamKIIα:Cre/R26$^{floxstop\text{-}TeNT}$ mice

GCs of CamKIIα:Cre/R26$^{floxstop\text{-}TeNT}$ (Cre/TeNT) and control (Cre) mice were tagged *in vivo* with AAV2.2 DIO-mGFP.

(A) Diagram depicting a simultaneous Cre-inducible expression of TeNT and mGFP.

(B) Images of mGFP-labeled GCs (top) and reconstructed dendritic trees of isolated neurons (bottom).

(C) Quantitative analysis of dendrite morphologies. *N*≥4 mice/19 neurons per genotype. Trees, P=0.66; Nodes, P=0.48; Tree length, P=0.92; Segment length, P=0.63.

(D) Enlarged fragments of GC dendrites.

(E) Superimposed samples of sEPSCs and sIPSCs recorded from mGFP-positive GCs in the presence of corresponding GABA and AMPA/NMDA receptor blockers. Vm was −70 mV.

(F) Relative abundances of distinct spine types on GC dendrites. Control, *N*=4 mice/15 neurons/1921 spines; TeNT, *N*=4 mice/19 neurons/1741 spines. T=thin, P=0.09; M=mushroom, P=0.07; S=stubby, P=0.5; O=other, P=0.7.

(G) Cumulative histogram analysis of sEPSC and sIPSC amplitudes. sIPSCs: *N*=3 mice/14–15 neurons/genotype, P=0.6; sEPSCs: Control, *N*=6 mice/20 neurons; TeNT, *N*=4 mice/12 neurons, P=0.88.

(H) Images of GC axons (top) and isolated LMTs (bottom) in the CA3.

(I) Densities of LMTs per axon length. *N*=3 mice/genotype, P>0.05.

(J) Numbers of LMTs of different sizes in the CA3. *N*=3 mice/genotype, P>0.05.

See also Figure S2 and Table S2.

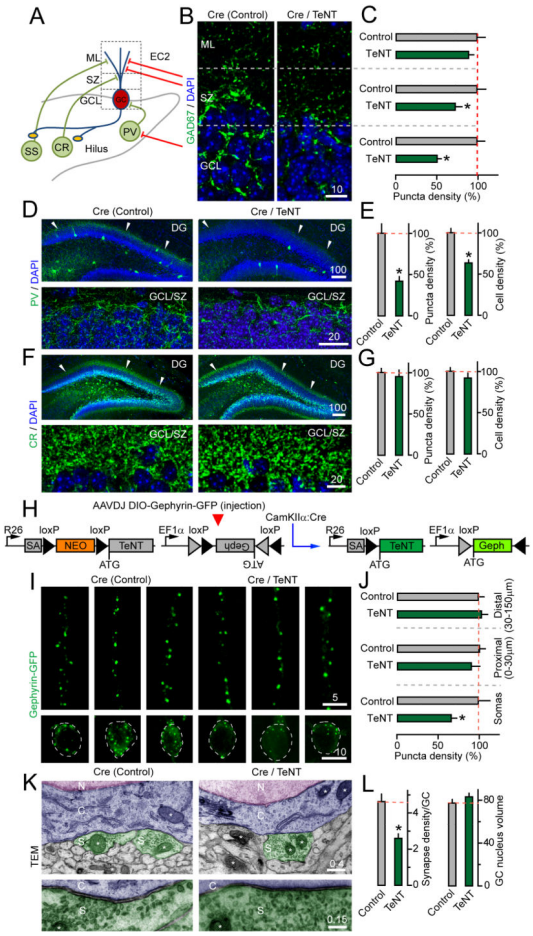

Figure 3. Loss of inhibitory synapses from GC somas in CamKIIα:Cre/R26$^{floxstop\text{-}TeNT}$ mice

Distribution of markers of GABAergic neurons and their synapses was examined in P14 CamKIIα:Cre/R26$^{floxstop\text{-}TeNT}$ mutants (Cre/TeNT) and their control littermates (Cre) by confocal and transmission electron microscopy (TEM).

(A) A simplified diagram of interneuron connectivity in the DG.

(B) Images of presynaptic terminals labeled in the DG with an antibody against GAD67. DAPI stains GC somas.

(C) Densities of GAD67-positive puncta in the ML, SZ and GCL. *N*=3 mice/genotype. ML, P=0.24; SZ, P<0.05; GCL, P<0.001.

(D) Images of the entire DG (top) and GCL/SZ (bottom) in sections stained with DAPI and an antibody against PV.

(E) Densities of PV-immunoreactive puncta in the GCL/SZ and neuronal somas across the DG. *N*=8 mice/genotype, P<0.001.

(F) Images of whole DG (top) and GCL/SZ (bottom) in sections labeled with DAPI and an antibody to CR.

(G) Densities of CR-positive puncta in the GCL/SZ and neuronal somas throughout the DG. *N*=3–4 mice/genotype. Axon puncta density in SZ, P=0.65. Cell density, P=0.25.

(H) Cre-inducible tagging of inhibitory postsynaptic sites with AAVDJ DIO-Gephyrin-GFP.

(I) Images of gephyrin-GFP fluorescence in dendrites (top) and somas (bottom) of isolated GCs.

(J) Densities of gephyrin-GFP puncta in dendrites and somas. *N*=3 mice/11–14 neurons/genotype. Distal dendrites, P=0.62; Proximal dendrites, P=0.39; Somas, P<0.02.

(K) TEM micrographs of inhibitory synapses on GC somas. N=nucleus; C=cytoplasm; S=synapse. Asterisks mark mitochondria.

(L) Numbers of somatic inhibitory synapses per section and GC nuclear volumes (as a control) in the GCL. *N*=3 mice/30 neurons per genotype, P<0.001.

See also Figure S3.

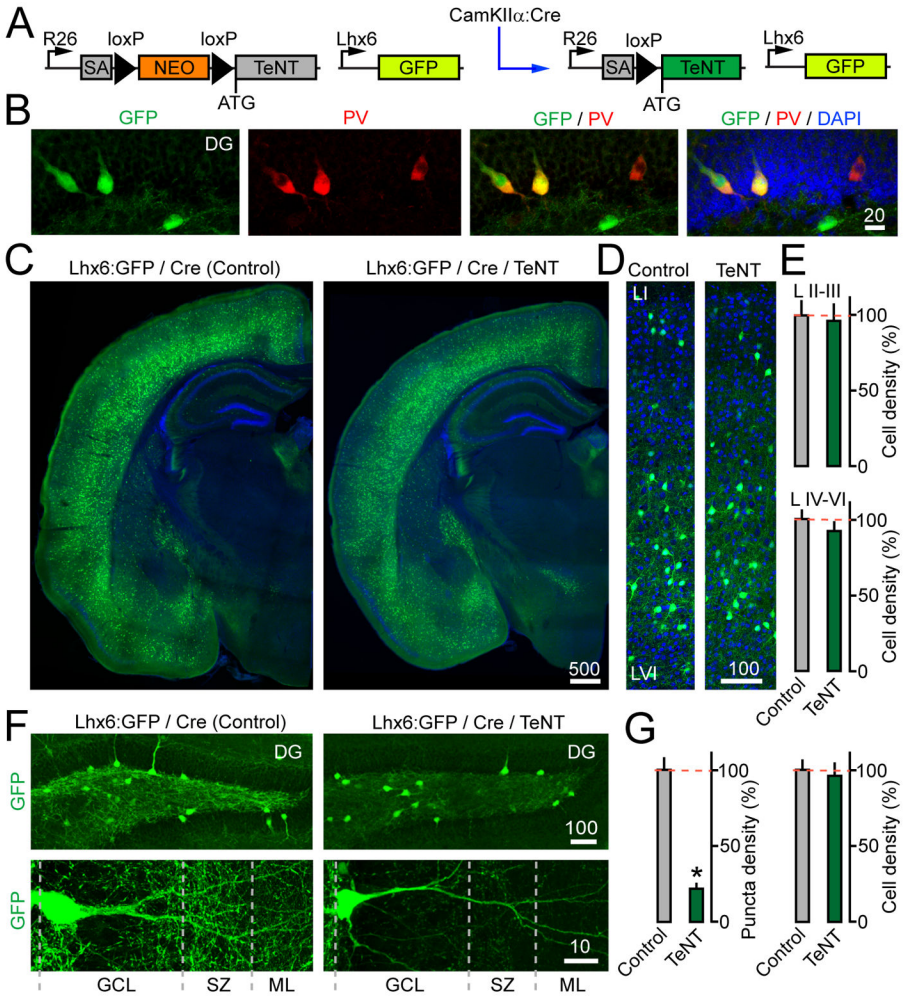

Figure 4. CamKIIα:Cre/R26$^{floxstop\text{-}TeNT}$ mice have reduced axon brunching of Lhx6-positive interneurons

(A) Schematic representation of mice carrying CamKIIα:Cre, R26$^{floxstop\text{-}TeNT}$ and Lhx6:GFP.

(B) Brain sections from Lhx6:GFP mice were stained with DAPI and an antibody to PV. Images of the DG are shown.

(C–D) Distribution of MGE-derived interneurons across the forebrain (panel C) and cortical columns (panel D).

(E) Numbers of Lhx6:GFP-tagged interneurons in superficial and deep layers of the somatosensory cortex. *N*=3 mice/genotype. P=0.76 and 0.42 for layers II–III and IV–VI, respectively.

(F) Images of Lhx6:GFP-expressing interneurons in the DG (top) and their processes in the GCL, SZ and ML (bottom) at P14. The boundaries of the GCL were identified based on DAPI staining (not displayed)

(G) Densities of Lhx6:GFP-positive axon puncta in the GCL/SZ and cell bodies throughout the DG. *N*=3 mice/genotype. Puncta density, P<0.001; Cell density, P=0.56.

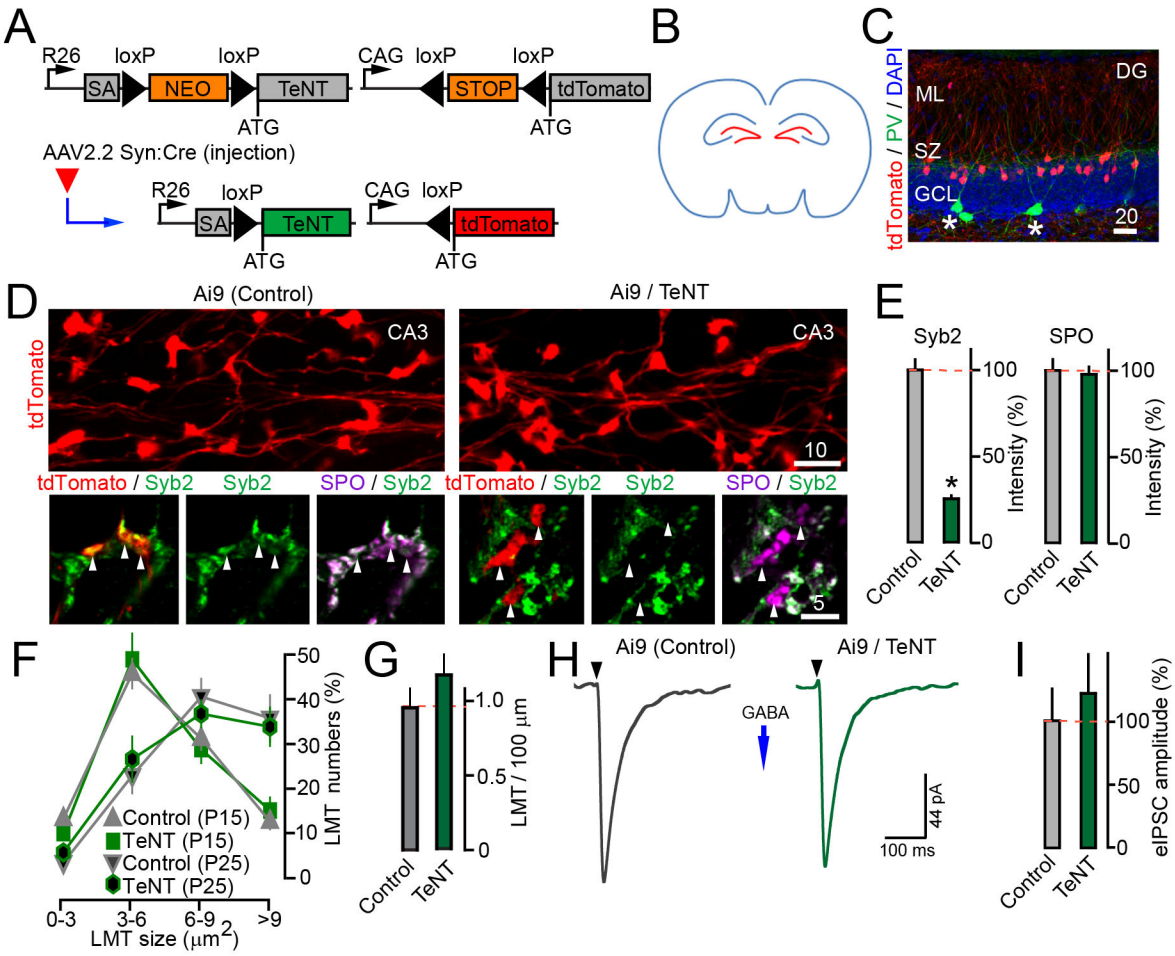

Figure 5. Loss of vesicular release from GCs does not disrupt their axon targeting and GABAergic inhibition

(A) AAV2.2 Syn:Cre-inducible expression of tdTomato and TeNT from Ai9 and R26$^{floxstop\text{-}TeNT}$ alleles.

(B–I) P1 mice carrying the Ai9 and R26$^{floxstop\text{-}TeNT}$ alleles (Ai9/TeNT) or Ai9 alone were injected with viruses into both cerebral lateral ventricles to selectively target GCs (as shown in panel B). Animals were analyzed at either P14 or P25.

(C) Specificity of recombination in the DG, as assessed by reporter induction. Brain sections from P14 Ai9 mice were stained with DAPI and an antibody against PV. Asterisks mark interneurons.

(D) Top: Tagged GC axons and their LMTs in the CA3 at P25. Bottom: Isolated LMTs labeled with antibodies to Syb2 and SPO. Asterisks mark the terminals of SNARE-deficient neurons.

(E) Averaged Syb2 and SPO staining intensities per LMT in the CA3. *N*=2 mice/genotype. Syb2, P<0.001; SPO, P=0.89.

(F) Numbers of tdTomato-positive LMTs of different sizes in the CA3. *N*=3 mice/genotype/age, P=0.28.

(G) Densities of LMTs per axon length at P25. *N*=3 mice/genotype, P>0.05.

(H) Samples of evoked IPSCs monitored from tdTomato-tagged GCs at P14 in response to stimulation of the GCL. Vm was −70 mV.
(I) Averaged IPSC amplitudes. *N*=2 mice/5–8 neurons/genotype, P=0.34.
See also Figure S4 and Tables S1–2.

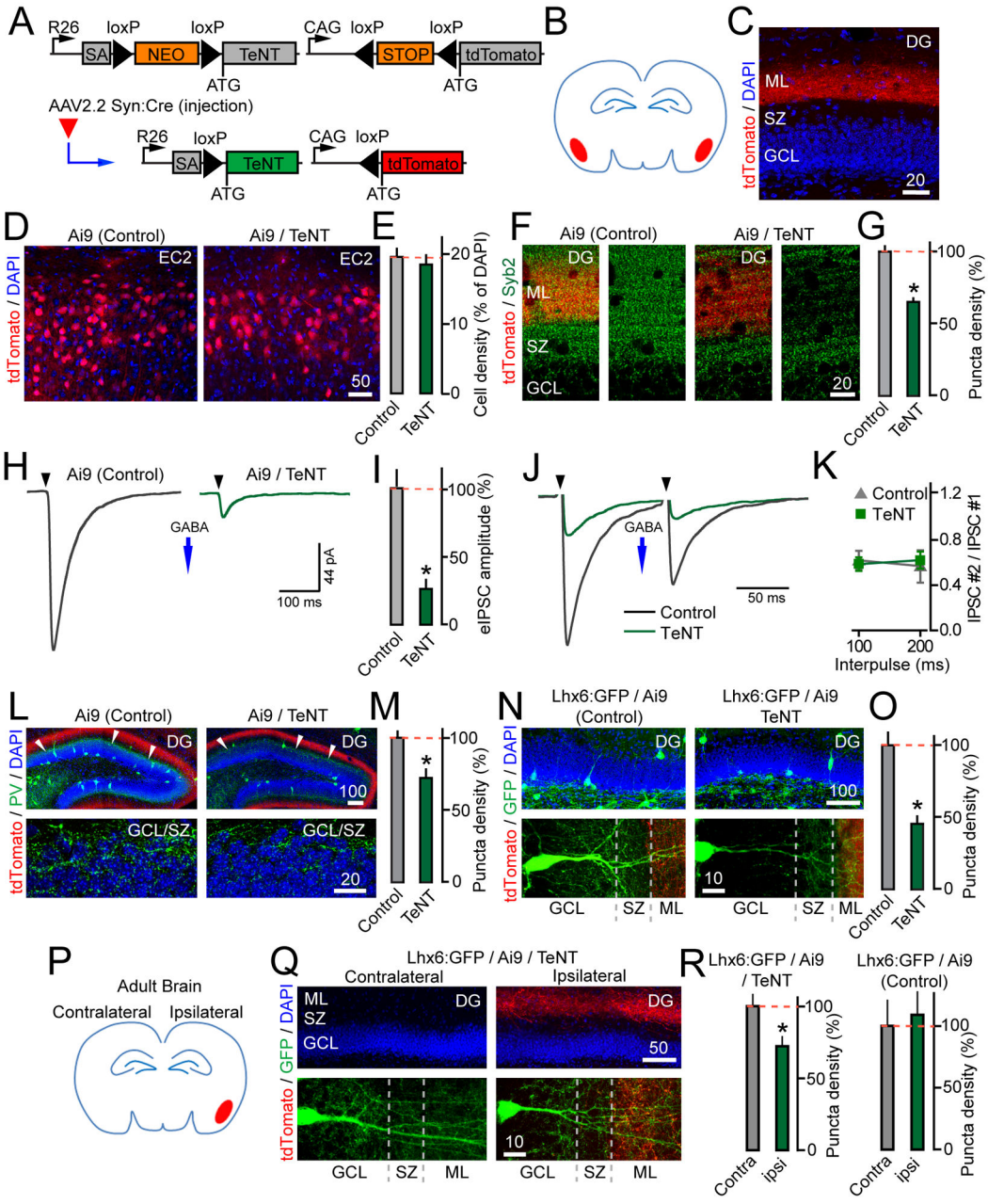

Figure 6. Axon branching of dentate Lhx6-positive interneurons is regulated by inputs from EC

(A) AAV2.2 Syn:Cre-inducible expression of tdTomato and TeNT from Ai9 and R26$^{floxstop\text{-}TeNT}$ alleles.

(B–O) P1 Ai9/R26$^{floxstop\text{-}TeNT}$ (Ai9/TeNT) and control Ai9 mice were bilaterally injected with viruses into the EC to target projection cortical neurons (as shown in panel B). All experiments were performed at P14.

(C) Images of tdTomato-positive axons of EC neurons in the ML of the DG. DAPI labels GC somas.

(D) Induction of tdTomato expression in the EC2.

(E) Recombination efficiencies of AAV2.2 Syn:Cre in the EC2, expressed as a fraction of cells with detectable tdTomato. *N*=3 mice/genotype, P=0.59.
(F) Images of the GCL/SZ/ML in sections labeled with an antibody against Syb2. GCL was identified by DAPI staining (not displayed).
(**G**) Density of Syb2-immunoreactive puncta in the ML. *N*=4 mice/genotype, P<0.001.
(H) Samples of evoked IPSCs recorded from GCs upon extracellular stimulation of the GCL. Vm was −70 mV.
(I) Summary graphs of eIPSC amplitudes. *N*=2 mice/8–9 neurons per genotype, P<0.02.
(J) Traces of evoked IPSCs elicited by 2 action potentials at 10 Hz.
(K) IPSC paired pulse ratios at 5 and 10 Hz. *N*=2 mice/3 neurons/genotype.
(L) Images of the entire DG (top) and GCL/SZ in brain sections stained with DAPI and an antibody to PV. Red fibers are axons of EC2 neurons. Asterisks mark the area of GCL where basket cells innervate GCs.
(M) Densities of PV-positive axon puncta in the GCL/SZ. *N*=3 mice/genotype, P<0.001.
(N) Images of whole DG (top) and GCL/SZ/ML (bottom) in sections isolated from EC-injected Ai9/R26$^{floxstop\text{-}TeNT}$ and Ai9 mice carrying the Lhx6:GFP allele.
(O) Densities of Lhx6:GFP-positive axon puncta in the GCL/SZ. *N*=3 mice/genotype, P<0.001.
(P–R) Lhx6:GFP/Ai9/R26$^{floxstop\text{-}TeNT}$ and Lhx6:GFP/Ai9 mice were injected with AAV2.2 Syn:Cre into one cortical hemisphere at P60 (as depicted in panel P). Interneurons were imaged in ipsilateral and unaffected contralateral areas of the DG two weeks later.
(Q) Top: Validation of the virus targeting specificity (GFP signal not shown). Bottom: Images of Lhx6:GFP-positive interneurons in contra- and ipsilateral sides of the DG.
(R) Densities of Lhx6:GFP-positive axon puncta in the GCL/SZ of contra- and ipsilateral DG. *N*=3 mice/genotype/group. TeNT, P<0.05; Control, P=0.74.
See also Figure S5.

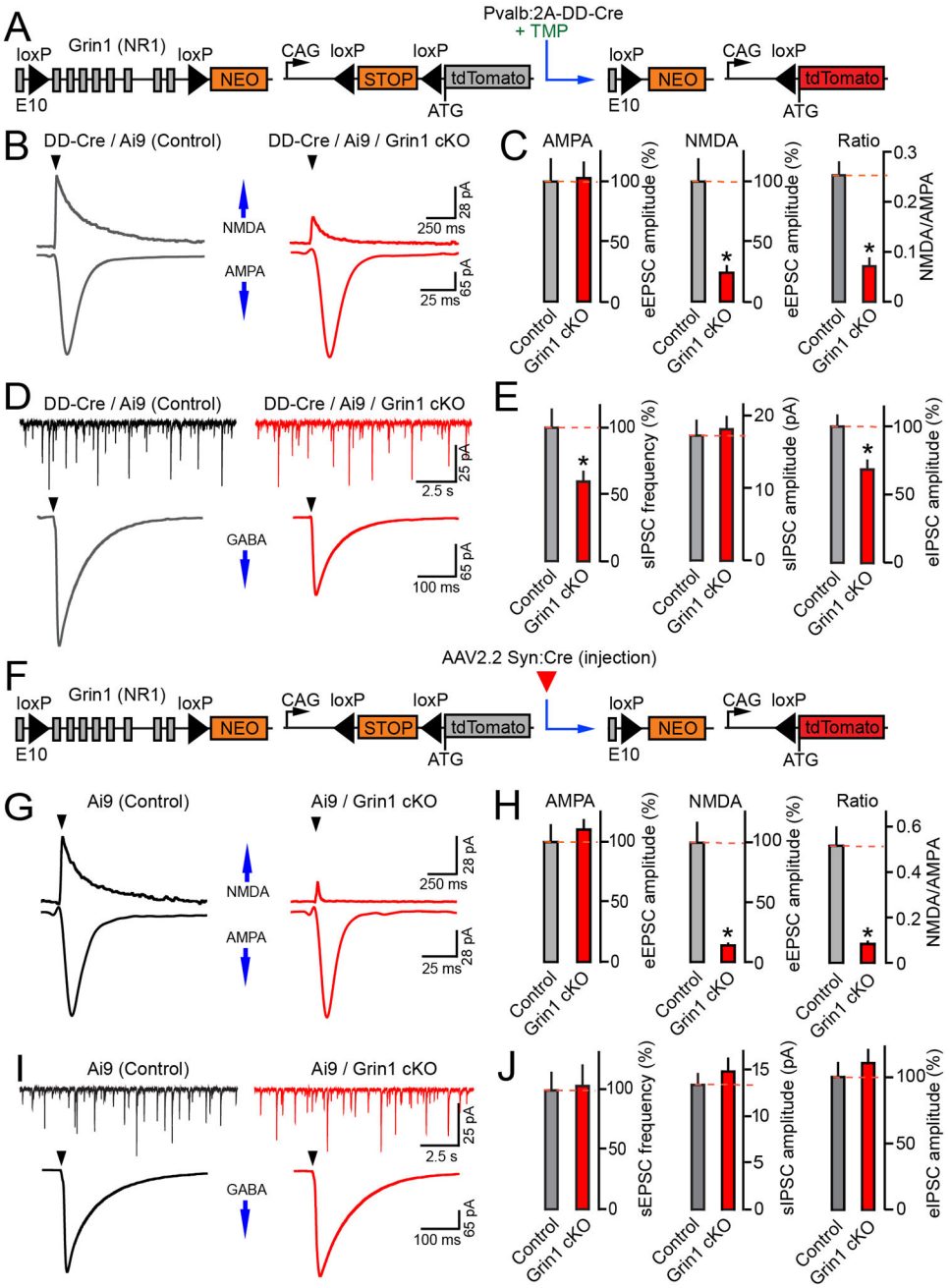

Figure 7. Synaptic transmission in the DG of mice deficient for NMDA receptors in PV neurons or GCs

(A–E) Grin1 was knocked out (cKO) in PV neurons. Pvalb:2A-DD-Cre/Ai9/Grin1$^{flox/flox}$ mice and their Pvalb:2A-DD-Cre/Ai9/Grin1$^{wt/wt}$ littermates were treated at P9–11 with TMP (0.3 mg/gm body weight/dose), which triggers recombination by stabilizing DD-Cre (as shown in panel A). Whole-cell recordings were performed in acute brain slices isolated at P25.

(B) Samples of AMPA- and NMDA-type eEPSCs recorded from tdTomato-positive interneurons in the DG in response to stimulation of the performant path. Vm was −70 and + 40 mV for AMPA- and NMDA currents, respectively.

(C) Mean eEPSC amplitudes and NMDA/AMPA ratios in PV cells. *N*=3 mice/7–9 neurons/genotype. AMPA, P=0.88; NMDA, P=0.001; NMDA/AMPA ratio, P<0.001.

(D) Traces of sIPSCs and eIPSCs monitored from untagged GCs. Evoked responses were elicited by stimulation of the GCL. Vm was −70 mV.

(E) Averaged sIPSC rates and sIPSC/eIPSC amplitudes in GCs of control and PV neuron-specific Grin1 cKO mice. *N*=3 mice/13–15 neurons/genotype. sIPSC frequency, P<0.02; sIPSC amplitude, P=0.77; eIPSC amplitude, P<0.01.

(F–J) P1 Ai9/Grin1$^{flox/flox}$ and control Ai9/Grin1$^{wt/wt}$ mice were injected into the cerebral lateral ventricles with AAV2.2 Syn:Cre to knock out Grin1 in GCs (as shown in panel F). Whole-cell recordings were performed from tdTomato-tagged GCs at P16–17.

(G) Samples of AMPA- and NMDA-type eEPSCs evoked by stimulation of the performant path. Vm was −70 and +40 mV.

(H) Mean eEPSC amplitudes and NMDA/AMPA ratios. *N*=2–4 mice/10 neurons/genotype. AMPA, P=0.77; NMDA, P<0.001; NMDA/AMPA ratio, P<0.001.

(I) Samples of sIPSCs and eIPSCs. Evoked responses were triggered by stimulation of the GCL. Vm was −70 mV.

(J) Summary of GC inhibition. Mean sIPSC rates and sIPSC/eIPSC amplitudes are shown. *N*=4 mice/13–14 neurons/genotype. sIPSC frequency, P=0.87; sIPSC amplitude, P=0.44; eIPSC amplitude, P=0.45. See also Figures S6–8 and Table S1.

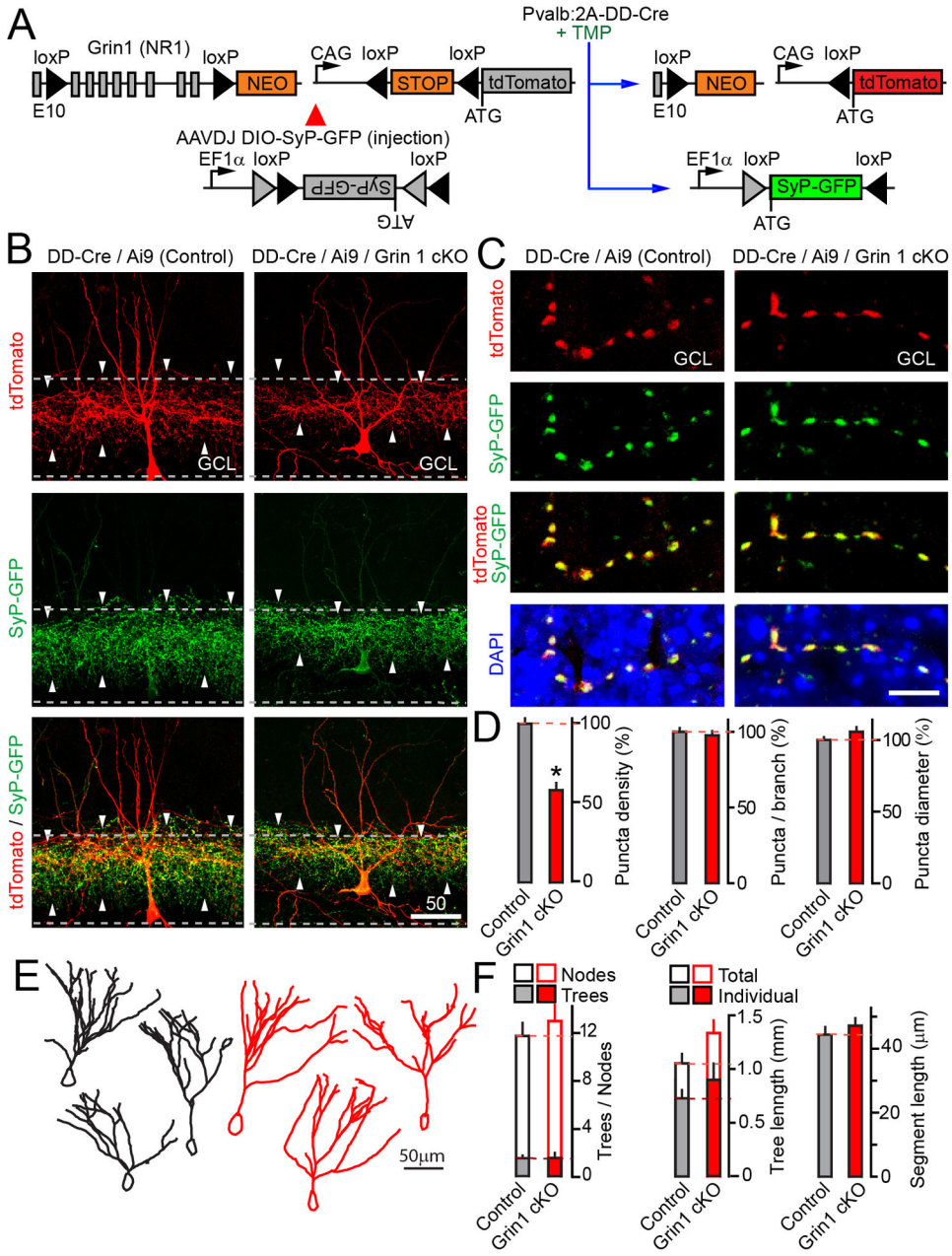

Figure 8. NMDA receptor-deficient PV neurons have reduced presynaptic networks

(A) Simultaneous TMP-inducible Grin1 cKO and expression of two fluorescent reporters in PV neurons.

(B–F) Newborn Pvalb:2A-DD-Cre/Ai9/Grin1$^{flox/flox}$ and Pvalb:2A-DD-Cre/Ai9/Grin1$^{wt/wt}$ mice were injected into the cerebral lateral ventricles with AAVDJ DIO-SyP-GFP. Sparse recombination was triggered with a single TMP pulse at P9 (0.3 mg/gm, as depicted in panel A). Morphologies of PV neurons in the DG were analyzed at P25.

(B) Images of PV cells expressing tdTomato and synaptophysin-GFP. Dashed lines mark the GCL (based on DAPI staining, not displayed).

(C) Images of presynaptic boutons formed by single axon segments in the GCL.

(D) Total densities of axonal/presynaptic puncta in the GCL, linear puncta density per axon branch, and puncta diameters. Total density: Control, *N*=10 mice/24 neurons; cKO, *N*=4 mice/12 neurons, P=0.001. Linear density and diameters: *N*=2 mice/7–9 neurons/genotype, P=0.53 and 0.12, respectively.

(E) Examples of reconstructed dendritic trees.

(F) Analysis of dendrite morphologies. Control, *N*=8 mice/24 neurons; cKO, *N*=4 mice/12 neurons. Trees, P=0.92; Nodes, P=0.49; Dendrites, P=0.27; Segments, P=0.46.

See also Table S2.